8-1-2009

Chip-Scale Nanophotonic Chemical and Biological Sensors Using CMOS Process

Lincoln Bollschweiler
Boise State University

Alex English
Boise State University

R. Jacob Baker
Boise State University

Wan Kuang
Boise State University

Zi-Chang Chang
National Chiao Tung University

See next page for additional authors

 DOI: 10.1109/MWSCAS.2009.5235915

Authors
Lincoln Bollschweiler, Alex English, R. Jacob Baker, Wan Kuang, Zi-Chang Chang, Ming-Hsiung Shih, and William Knowlton

Chip-Scale Nanophotonic Chemical and Biological Sensors using CMOS Process

Lincoln Bollschweiler, Alex English, R. Jacob Baker, *Senior Member, IEEE*, Wan Kuang, Zi-Chang Chang, Ming-Hsiung Shih, William B. Knowlton, William L. Hughes, Jeunghoon Lee, Bernard Yurke, Nankyung Suh Cockerham, Vance C. Tyree

***Abstract*— A monolithic integrated chip-scale surface plasmon resonance (SPR) sensor is demonstrated. The device consists of a *pn* photodiode covered with a periodic modified thin metal film whose lattice constant is on the order of the wavelength of light. The device performs real-time measurement of resonant wavelengths of enhanced optical transmission due to surface plasmon resonance, which are influenced by the presence of chemical or biological materials at the device's surface.**

***Index Terms* — surface plasmon polariton, photodiode, sensor, CMOS transimpedance amplifier**

I. Introduction

Surface plasmon resonance (SPR) sensing has become a central tool for characterizing and quantifying bimolecular interactions in life science and pharmaceutical lab research [1]. An SPR sensor typically consists of three integral parts: an SPR sensing element, an optical input/output coupler, and a photodetector followed by an image processing system. There has been an increasing demand for miniaturized SPR sensors beyond the current efforts, which have been primarily focused on packaging the photodetectors and the imaging processing systems [2]. In this paper, a monolithic integrated solution is demonstrated where the SPR sensing, electric current generation, and signal processing are achieved on the same plane. This in-plane approach offers the potential of miniaturization for minimal size and power consumption. It is an attractive choice for optical chemical and biochemical sensing because of the significant reduction in required resolution as compared to the traditional sensor-optics-detector counterparts. For the semiconductor industry, this solution expands the traditional CMOS core competency to diverse sensing applications.

This work was supported in part by DARPA MTO Office and administered by SPAWAR SYSCEN/San Diego under Contract #N66001-05-1-8911. Any opinions, findings, and conclusions or recommendations expressed in this publication are those of the author and do not necessarily reflect the views of DARPA or the Space and Naval Warfare Systems Center.

Lincoln Bollschweiler, Alex English, Jake Baker, Wan Kuang, William B. Knowlton, William Hughes, Jeunghoon Lee, and Bernard Yurke are with Boise State University, Boise, ID 83725 (corresponding author's e-mail: jbaker@ boisestate.edu).

Zi-Chang Chang and Min-Hsiung Shih are with National Chiao-Tung University, Taiwan, ROC. Min-Hsiung Shi is also with Academia Sinia, Taiwan, ROC.

Nankyung Suh Cockerham and Vance Tyree are with the MOSIS Service, Information Science Institute, University of Southern California, Marina del Rey, CA 90292

Surface plasmons (SPs) are surface electromagnetic waves that are trapped at the metal-dielectric interface due to their interaction with the valence electrons of the conductor [3]. In this interaction, the electrons respond collectively by oscillating in resonance with the incident light wave. The appeal of surface plasmon resonance for sensors arises from the large electromagnetic field enhancement at the metal surface, which leads to an increased light-matter interaction [4]. Any slight change in the refractive index within the range of the plasmon field causes a substantial change in spectral transmission. Outside the metal, the field intensity decays exponentially away from the metal surface within approximately a wavelength. This reduces the interference to measurements due to the materials of similar refractive index but lack of receptor binding.

Figure 1 shows the schematic of the chip-scale SPR sensor. An Ag film is deposited over the *p-n* photodiode. The periodic structures are then patterned onto the metal film. The sensor is illuminated by a collimated light from the top at a normal angle. When appropriate biological materials are attached to the receptors, surface plasmon resonance occurs on the Ag film. This leads to an enhanced optical transmission. The identification of chemical material is reflected as an increase of photocurrent.

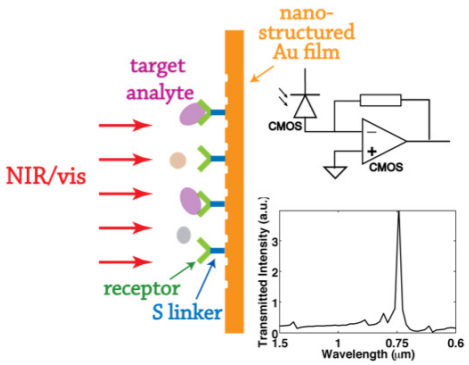

Figure 1 Schematics of a chip-scale nanophotonic biosensor integrating an SPR photonic sensor onto a photodiode. The inset shows the calculated optical transmittance of a corrugated Ag film.

The paper is organized as follows. In section II, the layout of the device is described. The device is fabricated through the MOSIS fabrication service on its AMI 0.5 μm C5 process [5]. The photodiodes and transimpedance amplifiers are characterized and discussed in Section III. In section IV, the spectral response of SPR sensors is measured and analyzed. The results are summarized in Section V.

978-1-4244-4480-9/09/$25.00 ©2009 IEEE

II. Layouts

A. Photodiodes

Sheets of *n*-type material were laid out on top of *p*-type substrate in order to maximize the area of the depletion region exposed to incident light. Examples of these layouts (created with Electric VLSI Design System software) can be seen in Figure 2. Diodes are laid out with either *n*-well or n^+ regions, providing a variation in the amount of doping in the *n*-type side, thereby affecting the width of the depletion region. Devices with metal-to-active contacts which segment the diode are designed, providing shorter paths for electron-hole pairs to propagate before reaching a low impedance metal. As seen in Figure 2, a layer of metal surrounds the active area, serving as a light-blocking aperture.

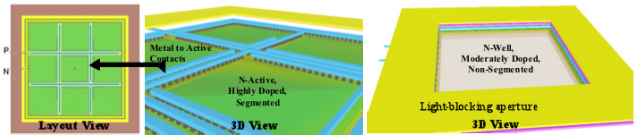

Figure 2 Layout and 3D views of photodiode designs. Both segmented (left and center) and non-segmented (right) designs were used on the chip. Additionally, both n^+ to *p*-substrate (green) and *n*-well to *p*-substrate (gray) photodiodes were fabricated on the chip.

B. Transimpedance Amplifiers

In order to transform the PD's photo-generated current into a readable voltage level, transimpedance amplifiers have been employed and fabricated on the same chip as the photodiodes. The chip under characterization has one amplifier for every PD. Figure 3 shows the optical image of the chip and Figure 4 is the layout of an amplifier. The amplifiers cannot be seen in the optical image because they are covered with a light blocking metal layer.

C. Full Chip

The full chip design and optical micrograph are shown in Figure 3. The PDs range in size from 40 µm up to 120 µm on a side for a total of 5 sizes. There are four varieties, *n*-well to *p*-substrate segmented and un-segmented and n^+ to *p*-substrate segmented and un-segmented. The segmented versions have metal to active contacts running through the PDs active area in attempt to provide shorter paths for photo-generated electron-hole pairs to travel before reaching low impedance metal lines. The smallest PDs (40 µm) do not have segmented versions. There are 18 different diode variations and this set is repeated on the chip 3 times, for a total of 54 PDs.

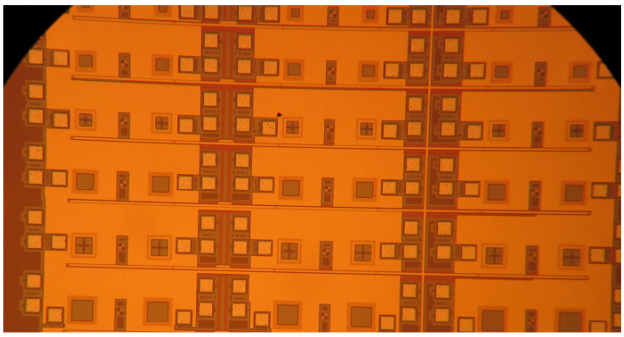

Figure 3 Optical micrograph of fabricated device. The transimpedance amplifiers are unseen in the image due to being covered by a light blocking metal layer.

III. Photodiode Characterization

A. Spectral Response of p-n Diode

Figure 5 shows the spectral responsivity of three bare PDs in the wavelength range of 410 and 1000 nm. The unpackaged chip is glued to a printed circuit board (PCB) and wire bonds are made to the PD's bonding pads. A subminiature version A (SMA) end launch was soldered to the PCB. The SMA cable is fed to a Stanford Research SR 445A 350 MHz preamplifier, which in turn is sent to a boxcar averager / integrator, which is finally connected to a voltmeter for measurement. To generate a photocurrent, a tunable-wavelength, pulsed laser is guided at a normal incidence onto the PDs. The laser produces a single wavelength of collimated light at a frequency of 10 Hz with an

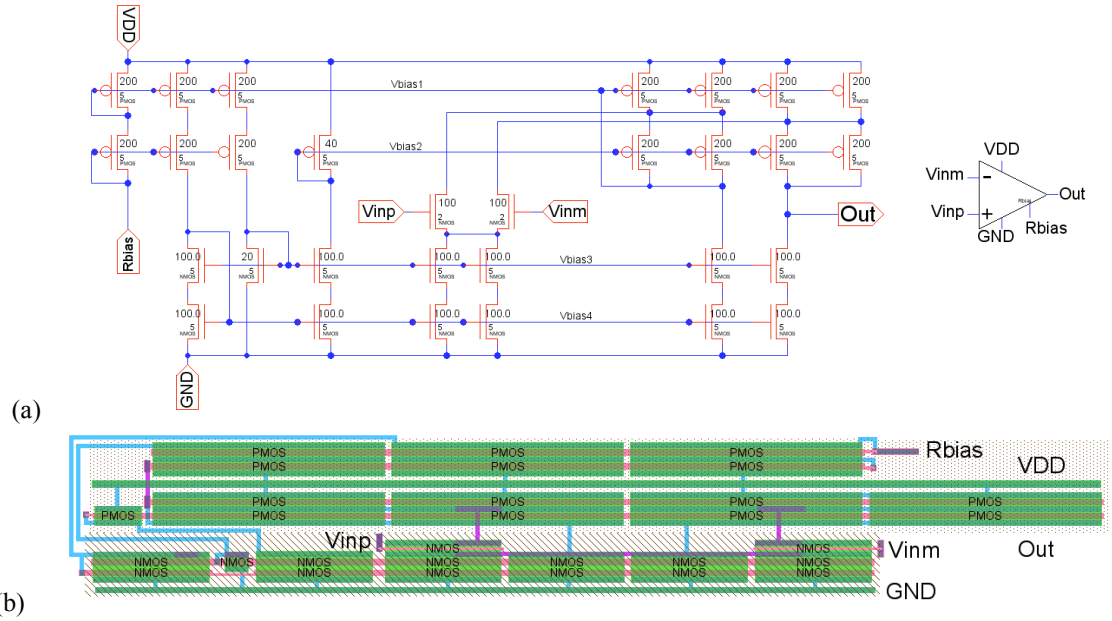

Figure 4 The schematics (a) and layout (b) of transimpedance amplifier

approximate 5ns pulse width. This duty cycle of $1x10^{-6}$% gave the PD ample time to fully discharge all of its photocurrent during each pulse. The boxcar integrator integrates the amount of area under this decay curve and produces an averaged voltage over a specified temporal window.

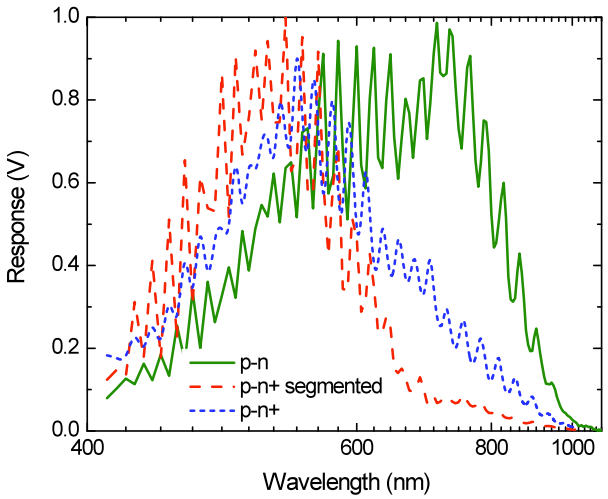

Figure 5 Spectral response of three photodiodes: *n*-well to *p*-substrate (segmented), n^+ to *p*-substrate (segmented), and n^+ to *p*-substrate (unsegmented). The induced photocurrent is amplified by a Stanford Research SR 445A preamplifier. The horizontal axis is inversely scaled.

Figure 5 shows that periodic oscillations in spectral response can be observed for all three PDs. This oscillation is due to the Fabry-Perot interference as a result of multi-layer dielectric stack (overglass) deposited on top of Si photodiodes. In a simplified air-dielectric-Si three-layer model, the incident light experiences multiple reflections at the air-dielectric and dielectric-Si interfaces. The transmitted power, T, can be described by,

$$T = 1 - \left| r_{01} - \frac{r_{12} t_{01} t_{10} e^{-2in_1 k_0 d}}{1 - r_{12} r_{10} e^{-2in_1 k_0 d}} \right|^2 = 1 - \left| r_{01} - \frac{r_{12} t_{01} t_{10} e^{-in_1 k_0 d}}{(1 + r_{12} r_{10}) \sin n_1 k_0 d + (1 + r_{12} r_{10}) \cos n_1 k_0 d} \right|^2 \quad (1)$$

where r_{01} is the Fresnel reflection coefficient for normal incidence from medium 0 (air) to medium 1 (dielectric), $r_{01} = (n_0 - n_1)/(n_0 + n_1)$. Similarly, r_{10} is the reflection coefficient for normal incidence from dielectric to air. t_{01} and t_{10} are the corresponding transmission coefficients. k_0 is the wave number in vacuum, $k_0 = 2\pi/\lambda_0$. d is the physical thickness of the dielectric layer. Equation (1) reaches a minimum when the denominator of the equation becomes zero.

$$(1 + r_{12} r_{10}) \sin n_1 k_0 d + (1 - r_{12} r_{10}) \cos n_1 k_0 d = 0 \quad (2)$$

or,

$$\sin(k_0 n_1 d + \phi) = 0 \quad (3)$$

where ϕ is given by $\tan\phi = (1 - r_{12} r_{10})/(1 + r_{12} r_{10})$. Equation (3) shows that the oscillation is periodic with respect to the wave numbers. Hence in Figure 5 where the wavelength axis is in inverse scale, an equal distance is observed between spectral peaks. From Eq. (3), the optical length of the dielectric medium can be estimated by,

$$n_1 d = \frac{\lambda_0^2}{\Delta\lambda} \quad (4)$$

in which, $\Delta\lambda$ is the wavelength spacing between the adjacent peaks in Figure 5, and λ_0 is the average of the two peak wavelengths. Equation (4) shows that the *optical* thickness of the overglass layer is approximately 2000 nm.

In addition, the *p-n* photodiode shows a higher responsivity at near infrared wavelengths compared with photodiodes with heavier *n* doping. It is partly a consequence of a larger depletion layer width. For short wavelengths, however, the degree of light absorption within the surface diffusion layer becomes very large. Therefore, *p-n*$^+$ photodiodes, which has a thinner diffusion layer and a closer distance to the *pn* junction, yield a higher the sensitivity at the shorter wavelength. A segmented photodiode further reduces the distance between the *pn* junction and the ohmic contact, resulting in a further improved responsivity at the short wavelength regime. However, the responsivity at longer, near infrared wavelengths suffers because of free electron absorption of the metal segments.

B. Transimpedance Amplifier

The on-chip transimpedance amplifiers are also characterized. They are covered beneath the optically opaque metal layer to prevent their change in amplification as a result of light incidence. The amplifiers are characterized for low-frequency circuits and the illumination for this measurement is generated from a Xe arc lamp filtered through a Newport Cornerstone 260 monochromator. For a *p-n*$^+$ photodiode which had a segmented active area, the measurements show that a transimpedance of 10^6 is achieved for all wavelengths of interest.

IV. SPP Photonic Sensor

Optical transmittance of a periodically textured Ag membrane demonstrates an extraordinary transmission due to surface plasmon resonance [6]. Numerical calculations show that this surface plasmon resonance is wavelength-, angle-of-incidence, polarization-, and refractive-index-dependent.

Figure 6 shows the scanning electron micrograph images of the Ag film after being periodically modified through electron-beam lithography and ion beam etching. The periodic array of holes on the Ag film is created by electron beam lithography and Ar+ ion beam etch. A 200 nm PMMA is spin coated on diode and subsequently patterned with electron beam. After the development, Ar+ ion beam etch transfers the patterns on PMMA mask to the 100 nm thick Ag film. The dimension of the periodic pattern is up to 300×300 μm, which is designed to cover the active area of the *pn* photodiodes. The Ag film has a thickness of 100 nm.

The transmission of the device was measured for wavelengths of 410 nm through 950 nm with samples taken at 5 nm intervals. A measurement was also performed for the transmission of the wafer on which the device was fabricated. The

response of the device was normalized by the response of the wafer, eliminating the spectral response of the optical components involved in the measurements. Figure 7 shows the optical transmission as a function of wavelength for three different lattice constants for normal incidence. In comparing with a uniform Ag film, a nanostructured Ag film shows an extraordinary transmission at certain optical wavelengths. This is attributed to surface plasmon resonance occurred at the Ag-air interface.

For Ag film periodically modified in a square lattice, the

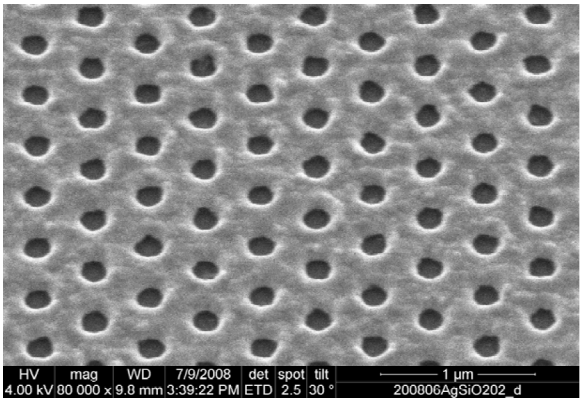

Figure 6 Scanning electron micrograph images of a nanostructured Ag film. The Ag film has a thickness of 100 nm. The distance between the adjacent holes (lattice constant) is 420 nm.

enhanced optical transmission occurs when the in-plane wave vector, $k_0 \sin\theta$, of light that has been scattered by one or more grating vectors matches the guided SPP mode at the Ag-dielectric interface. As a result, both the transmittance and reflectance of the film are modified. For a given wavelength, this can be expressed by momentum conservation condition,

$$\vec{k}_0 \sin\theta \pm m\vec{G}_1 \pm n\vec{G}_2 = \vec{k}_{spp} \qquad (5)$$

where k_0 is the wave vector of the light incident at a angle of θ, $\vec{G}_1$ and $\vec{G}_2$ are the reciprocal space vectors associated with the square lattice, and *m* and *n* are integers. The SPP mode at the Ag-dielectric interface has a propagation constant $k_{spp} = k_0\sqrt{\varepsilon_{Ag}\varepsilon_d/(\varepsilon_{Ag}+\varepsilon_d)}$, where ε_{Ag} and ε_d are the dielectric constant of Ag and overglass, respectively. This yields the wavelength of enhanced transmission,

$$\lambda_{spp} = \frac{a}{m^2+n^2}\sqrt{\frac{\varepsilon_{Ag}\varepsilon_d}{\varepsilon_{Ag}+\varepsilon_d}} \qquad (6)$$

Eq. (6) is an implicit equation for λ_{spp} because the metallic dielectric constant depends on wavelength. SPPs consistent with Eq. (6) are different in nature from that of an isolated hole because they occur at only certain discrete wavelengths. The SPPs on a periodically modified Ag film are best thought of as standing waves consistent with Bloch's theorem [7]. Figure 7 shows that the measured peaks transmission wavelengths are consistent with Eq. (6). As the lattice constant increases from 500 nm to 600 nm, the peak transmissions shift to longer wavelengths as indicated by the square brackets in the figure.

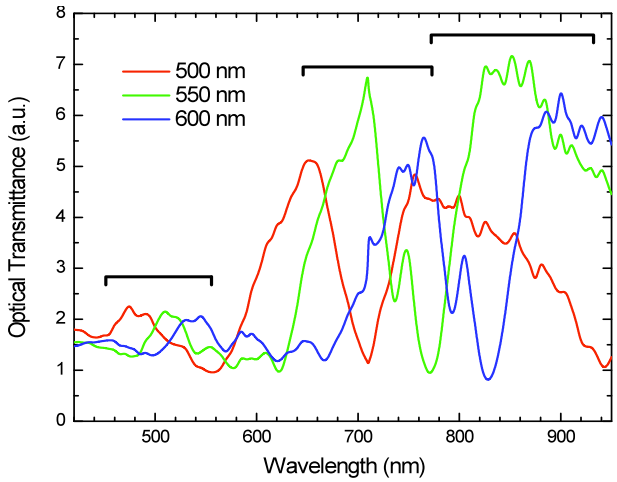

Figure 7 Optical transmittance of periodically modified Ag films in square lattice for normal incidence of light from 410 to 950 nm. The lattice constants of the Ag film are 500, 550, and 600 nm, respectively. The square brackets in the figure indicate the spectral shift due to the difference in lattice constants.

As can be seen from Eq. (6), the transmission peaks are also a function of the dielectric constant. As the nanoholes on Ag membrane are filled with chemical or biological materials under study, the peak transmission wavelengths change accordingly.

V. Conclusion

In summary, an integrated optical sensor is presented utilizing surface plasmon resonance on a periodically modified Ag film. The characterization of photodiodes, amplifier, and surface plasmon resonance demonstrates that the experimental results are consistent with expectations. It also shows that monolithic integration is a viable design platform for nanophotonic chemical and biosensors.

References

[1] *Optical Biosensors: Present and Future.* **Ligler, F. and Taitt, C.** 2002, Elsevier Science.

[2] **Pang, H., Likamwa, P. and Cho, H.** Tokyo : s.n., 2006. Proc. Inter. Conf. Micro Total Analysis Syst.

[3] **Raether, H.** *Surface Plasmons on Smooth and Rough Surfaces and on Gratings.* s.l. : Springer-Verlag, 1988.

[4] *Plasmonics: merging photonics and electronics at nanoscale dimensions.* **Ozbay, E.** 5758, 2006, Science, Vol. 311, pp. 189-193.

[5] *MOSIS Integrated Circuit Fabrication Service.* [Online] http://www.mosis.com.

[6] *Surface plasmon subwavelegth optics.* **Barnes, W. L., Dereux, A. and Ebbesen, T. W.** 2003, Nature, Vol. 424, pp. 824-830.

[7] *Playing tricks with light.* **Pendry, J.** 5434, 1999, Science, Vol. 285, pp. 1687-1688.